

# Experimental evidence of flow destabilization in a 2D bidisperse foam.

I. Cantat,\* C. Poloni, and R. Delannay  
 GMCM, UMR 6626, Université de Rennes (CNRS), 263,  
 av. du Général Leclerc 35042 Rennes Cedex, France  
 (Dated: February 6, 2008)

Liquid foam flows in a Hele-Shaw cell were investigated. The plug flow obtained for a monodisperse foam is strongly perturbed in the presence of bubbles whose size is larger than the average bubble size by an order of magnitude at least. The large bubbles migrate faster than the mean flow above a velocity threshold which depends on its size. We evidence experimentally this new instability and, in case of a single large bubble, we compare the large bubble velocity with the prediction deduced from scaling arguments. In case of a bidisperse foam, an attractive interaction between large bubbles induces segregation and the large bubbles organize themselves in columns oriented along the flow. These results allow to identify the main ingredients governing 2D polydisperse foam flows.

PACS numbers: 82.70.Rr, 83.50.Ha, 83.60.La

## I. INTRODUCTION

In the context of complex and structured fluids, 2D foam rheology gives rise to a revived interest. In these materials, the subtle interplay between the elastic, plastic and viscous behaviors induces complex rheological properties. The similarities between fluid foam, pastes, clays or slurries arise from the organisation at small scale of a disordered structure, that governs the macroscopic behavior. In case of foam, this small scale is the millimetric bubble scale, which is much easier to observe than the molecular scale usually involved. The structure determination is especially convenient in 2D foam which is thus often used as a model system for complex fluids [1, 2, 3, 4].

We developed an experimental set-up enabling foams to flow in a dissipative regime in a large 2D channel. The foam is confined between two horizontal glass plates separated by a small gap allowing a sole bubble layer to form. The whole films network, as well as the velocity fields, can thus be determined from images taken from above, where bubbles appear as polygons of various areas. Each vertical film touches both plates along lines called *Plateau borders*. When sliding on the plates, they induce a viscous dissipation that becomes important even at relatively small velocities [5, 6]. When a foam is pushed in the cell, it is thus submitted to a viscous force depending on its velocity and on the density of Plateau borders, *ie* on the bubble sizes. If the foam is polydisperse, the largest bubbles experience a smaller drag (per unit foam surface, in a 2D language) than the smallest ones and tend therefore to move faster than the mean flow. The resulting flow is difficult to quantify in the general case of a polydisperse foam. As a first step, we investigated the case of a single large bubble embedded in a sea of much smaller bubbles and the case of a bidisperse foam with a minority of large bubbles. These

large bubbles, that play the role of defects (or holes) in the foam, can be produced *a posteriori* with a controlled size and position by vaporisation of liquid films with a laser.

As in a viscous instability of an interface, the pressure gradient in the foam is higher in-front of the hole than to the sides. A similar hole in a simple viscous liquid would move ahead for this reason. In a foam, the shear stress created by the different pressure gradients must exceed a yield stress. A threshold velocity is thus set by a competition between surface tension and dissipative forces. Only above this velocity, the large bubbles begin to migrate through the smaller bubbles. This migration does not imply that films break : the process is based on elementary neighbors exchanges involving four bubbles called *T1* events [7](see Fig. 2). The flow destabilization presented in this paper is based on wall effects and should thus be more important at smaller scale and especially in the domain of microfluidics.

This enhanced role of the dissipation in 2D foam flows in presence of large bubbles has been predicted numerically but is experimentally evidenced here for the first time. We present the experimental set-up in the section 2 and the qualitative flow behavior in section 3. Then, in section 4, we briefly recall the theoretical predictions previously obtained in [8, 9]. The section 5 is devoted to the relative velocity of a single large bubble in a monodisperse foam flow, which is the main result of this paper. Finally, in section 6, we show that size segregation occurs in the case of several large bubbles and that these bubbles organize themselves in columns oriented in the direction of the flow.

## II. EXPERIMENTAL SET-UP

Foams were prepared from a solution of SDS (3g/L), dodecanol (0.01g/L) and glycerol (0.05 L/L) in ultra pure water. As-prepared solutions were used within a period of 24h. The surface tension is  $\gamma = 31 \cdot 10^{-3} \text{N/m}$  and the bulk viscosity is  $\eta = 1.1 \cdot 10^{-3} \text{Pa.s}$ . The cell flow is made

---

\*isabelle.cantat@univ-rennes1.fr

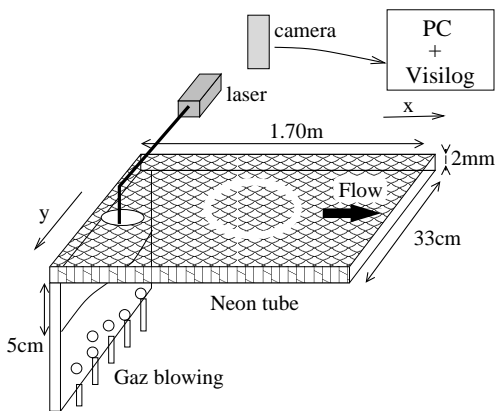


FIG. 1: Experimental set-up.

of two large horizontal glass plates ( $l = 35\text{cm} \times L = 170\text{cm}$ ) separated by a gap  $h = 2\text{mm}$  (fig. 1). It is connected upstream to a vertical production cell, of the same width and thickness, containing the foaming solution. The gap thickness is ensured by a steel piece, on which the glass plates are simply clamped. The foam is produced by blowing nitrogen continuously at a controlled flow rate through 4 equally spaced needles of diameter 1mm. It drains in the vertical cell until it reaches the main cell (fig.1). The present data were collected with a drainage height of 5 cm. The resulting liquid fraction is difficult to estimate but it corresponds to a very dry foam.

Depending on the gas flow rate we impose, the turbulence in the foaming solution is modified and yields various polydispersities. We worked with almost monodisperse foams with a typical bubble volume of  $V = 5 \cdot 10^{-2} \text{mL}$  (which gives a typical diameter of  $d = 5\text{mm} \pm 1$  for the polygons), obtained at the small flow rate of 1.5 mL/s per injector. The large bubble is produced by a YAG laser (wave length 1064 nm, energy per pulse 20 mJ, pulse duration 5 ns). The beam is successively focused on each desired film with an orientable lens, until a bubble 10 to 400 times larger in volume is produced. Once the foam and the defect are produced at low flux, the foam flow is accelerated at the required velocity by increasing the gas flow rate. Velocities were varied between  $0.3\text{cm/s}$  and  $10\text{cm/s}$ . The structure of the foam produced at this stage may be highly disordered but it does not influence the flow observed downstream.

The foam is lit laterally by a circular neon tube of diameter 0.4 m, put horizontally just below the cell on a black board. The Plateau border network reflects the light at  $90^\circ$  and thus appears from above in white on a black background (see Fig.2). Only the Plateau borders perpendicular to the incident light lead to a good contrast and the isotropy of the light is thus crucial. The camera is placed above the middle of the cell, and the large bubble shape has then time enough to relax spontaneously from its initial arbitrary shape before reaching the recording zone. We record 25 images per second with

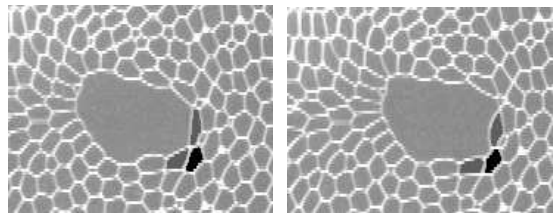


FIG. 2: Details of the raw images obtained from the camera. The foam, lit laterally by a circular neon tube, appears in white on black background. The mean flow is oriented to the right and the two images are separated by 120 ms. Small bubbles typical size is  $d=5\text{mm}$ . The large bubble is migrating through the smallest ones due to  $T1$  events : one of these elementary plastic transformations occurs between images (a) and (b) and the involved bubbles are underlined with a darker grey level.

a Pulnix TM6CN camera, with a resolution of  $570 \times 760$  pixels. Images are processed using a commercial software named Visilog to isolate each bubble and determine its area  $a$  and center of mass. The polygon area  $a$  is related to the bubble volume  $V$  through the relation  $V = ha$ . This 2D language will be used without precision in the following. The images treatment consists in the following operations : we subtract the background to remove the large scale heterogeneities of lightening and we get binary images by thresholding (liquid is white and gas black). Then a white pixel dilatation improves the bubble separation and the continuous white network thus obtained is skeletized to get finally a one pixel width continuous frontier around each black bubble. The last step is to record the area and the center of mass of these connex domains of back pixels. Bubble tracking between images  $n$  and  $n+1$  is then performed. A bubble  $k$  in image  $n$  is identified with the bubble  $k'$  in image  $n+1$  if its center of mass (computed in image  $n$ ) belongs to  $k'$  in image  $n+1$ . We checked manually the pairing method on few images and found that the error ratio was less than few percents, so the individual bubble trajectories are determined with a good precision.

The dissipation in the foam is mainly due to the viscous forces between the glass plates and the Plateau borders. The viscous force per unit Plateau border length is predicted by the lubrication theory to be  $\mathbf{f}_v \sim -\gamma Ca^\alpha \mathbf{u}_x$ , with  $Ca = \eta v_0 / \gamma$  the capillary number,  $v_0 \mathbf{u}_x$  the Plateau border velocity and  $\alpha$  an exponent which is  $2/3$  in the limit of wet foam and mobile surfactants [5, 10] and that varies roughly between 0.5 and 0.7 in the general case [11]. For the present foaming solution and in the velocity range investigated, we measured  $\alpha = 0.5 \pm 0.05$  with the technique detailed in [6]. These viscous forces are simply balanced by the pressure field, which scales, in a monodisperse foam of typical bubble diameter  $d$ , as

$$P(x) \sim -x \gamma Ca^\alpha / (hd). \quad (1)$$

The total pressure gap  $\Delta P$  between upstream and downstream was measured with a pressure captor put in the foaming solution. For a flow velocity  $v_0 = 3.2 \cdot 10^{-2} \text{m/s}$

and a small bubble size  $d = 5 \cdot 10^{-3} m$ , we measured  $\Delta P = 2800$  Pa, leading the typical viscous force per unit length of Plateau border  $f_v = h\Delta P d / (2L) \sim 10^{-2} N/m$ , in good agreement with previously obtained data [6].

### III. QUALITATIVE BEHAVIOR

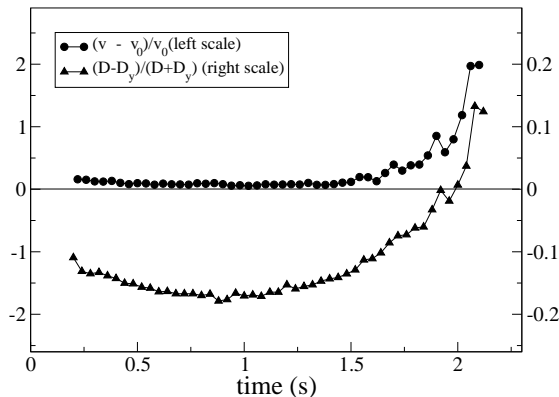


FIG. 3: The large bubble  $v$  is compared to the average flow velocity  $v_0$ , and correlated to the large bubble shape (the LB diameters in the  $x$  and  $y$  direction are respectively  $D$  and  $D_y$ ). An elongated shape oriented across the flow (large  $D_y$ ) gives rise to a stationary plug flow ( $0 < t < 1.5$ ). This shape may spontaneously destabilize ( $1.5 < t < 2$ ): a tip grows downstream in the flow direction, similarly to a viscous digitation. The tip finally contains the whole LB which is then oriented along the flow ( $t > 2$ ). This transformation coincides with an acceleration of the large bubble.

The flow is obtained with a controlled foam flux. At the velocity range we investigated, the first bubble layer on both sides slips on the wall at the mean velocity. In monodisperse foam, topological transformations are thus very rare and the foam structure remains almost unchanged during the flow. The instantaneous velocity distribution is well fitted by a Gauss distribution with a standard deviation of the order of  $\pm 5\%$ , due to the pixelisation. In contrast, in the presence of a large bubble, the plug flow becomes unstable above a given foam velocity. The large bubble velocity is then larger than the mean flow velocity  $v_0$ , with relatively large amplitude fluctuations and an orientation that may vary between  $\pm 30^\circ$  with respect to the mean flow direction (see Fig. 4). The large bubble shape was characterized by its diameters in the direction of the flow  $D(t)$  and in the transverse direction  $D_y(t)$ . These two parameters depend on time, in contrast with the LB area which is constant. The LB velocity is strongly correlated to the bubble elongation  $(D - D_y)/(D + D_y)$  that varies roughly between  $-1/2$  and  $1/2$ . The large bubble alternates periods during which it moves much faster than typical bubbles, with a shape

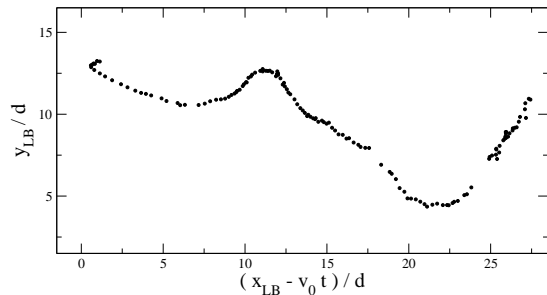


FIG. 4: Large bubble trajectory through the network of small bubbles. The position  $(x_{LB}, y_{LB})$  of the large bubble is measured in the frame moving with the mean velocity of the foam  $v_0 \mathbf{u}_x$ , in unit of small bubble diameter  $d$ . The foam velocity is larger than the velocity threshold and the large bubble moves in the  $x$  direction with a velocity fluctuating in amplitude and direction. Each dot corresponds to an image, separated by 40 ms.

elongated in the direction of its own relative motion, and periods during which it moves at the average speed with an elongated shape perpendicular to the mean flow (see Fig. 3).

The large bubble migration occurs without films breakages. Small bubbles are separated in front of the large bubble and are reconnected at the rear. These so-called T1 events, depicted on Fig. 2, are mainly localized very close to the large bubble, but many structure reorganisations are also induced much further, in the whole camera field. The velocity field around the large bubble may exhibit very different behaviors. Indeed, the presence of a wake of small bubbles behind the large one is intermittent. Comparison with foams flowing around an obstacle of fixed shape would thus be very interesting to perform [12].

### IV. THEORETICAL PREDICTIONS

This instability was already studied numerically and theoretically in [8, 9]. We summarized here the theoretical predictions for the large bubble velocity to improve the article self-consistency. The scaling behavior of the threshold is obtained from the expression of the various forces acting on the large bubble. From the pressure field given in eq. 1, we obtain the resulting pressure force on LB,

$$F_d \sim D^2(\gamma/d) Ca^\alpha, \quad (2)$$

which is the driving force for the LB migration. For sake of simplicity, we only retain in the model a single diame-

ter  $D$  for the large bubble. Below the threshold, the LB equilibrium thus results from a competition between the pressure field pushing LB downstream (the driving force  $F_d$ ) and the surface tension force of the soap films network that try to keep LB at its initial position in the foam frame. At small deformations, this force  $F_e$ , due to the fact that any modification of the foam structure increases the total amount of interfaces (and then of energy), is well predicted by a purely elastic model[13]. This leads to

$$F_e \sim \gamma h X / d, \quad (3)$$

with  $\gamma/d$  the order of magnitude of the foam shear modulus [7] and  $X$  the LB displacement with respect to its equilibrium position. This expression is obtained from a continuous incompressible 2D elastic medium at rest at infinity. In this case, the force exerted on a circular obstacle scales indeed as the obstacle displacement times the material shear modulus (up to disregarded logarithmic corrections in the obstacle size).

The local elastic stress  $\sigma$  is related to  $F_e$  by  $F_e = \sigma L_{geo} h$ , with  $L_{geo} h$  the typical area on which the stress is important around the front or the rear of LB. At the instability threshold, this local stress reaches the plastic threshold of the foam, scaling as  $\gamma/d$  [13]. The force balance on the large bubble is then, from eq. 2,  $D^2(\gamma/d) Ca^\alpha \sim \gamma L_{geo} h / d$  or, equivalently, with  $v_{th}$  the velocity threshold,

$$\eta v_{th} / \gamma \sim (h L_{geo} / D^2)^{1/\alpha}. \quad (4)$$

Above this threshold, the large bubble begins to migrate, with a mean velocity  $v$  modelised by the following process. The instantaneous LB velocity  $v(t)$  decreases during the elastic loading of the foam until the plastic threshold is reached. Then T1 events occur and a new cycle begins. A full stress relaxation is assumed after each plastic events and the elastic force is zero. Between two plastic events, the elastic force is obtained from eq. 3,  $F_e = \gamma h / d \int_0^t (v(t') - v_0) dt'$ . The integral is the LB displacement  $X$  with respect to the small bubble network, since the last plastic relaxation, occurring at  $t=0$ . The force balance is then

$$\frac{\gamma h}{d} \int_0^t (v(t') - v_0) dt' - \frac{D^2 \gamma}{d} \left( \frac{\eta v_0}{\gamma} \right)^\alpha + D \gamma \left( \frac{\eta v(t)}{\gamma} \right)^\alpha = 0, \quad (5)$$

the first term being the elastic force given above, the second one the driving force (eq.2) and the third one the excess of viscous force exerted around the large bubble that moves faster than the mean flow. This integral equation has been solved analytically in [9]. In the simple case  $\alpha = 1$  and  $D \gg d$  we obtain for the LB mean velocity  $v$  the expression given below. It differs only by few percents from the general expression, for reasonable values of  $\alpha$  and  $D/d$ , and will thus be used, for sake of simplicity (see Fig. 7).

$$\frac{v - v_0}{v_0 \frac{D}{d}} \sim \frac{-v_{th}/v_0}{\ln \left( 1 - \frac{v_{th}}{v_0} \right)}. \quad (6)$$

When  $v_0 \gg v_{th}$ , the expression becomes asymptotically  $(v - v_0)/(v_0 D/d) = 1$  or equivalently  $v = v_0 D/d$  with  $D \gg d$ . These equations 4 and 6 are used to rescale the experimental data.

## V. EXPERIMENTAL RESULTS

The aim of the present paper is to determine experimentally the relation, at each time, between the LB velocity in the flow direction, denoted by  $v(t)$ , the mean flow velocity  $v_0$  and the large bubble size characterised by its diameter in the x direction  $D(t)$ , which appeared to be the pertinent size parameter.

We analyzed 56 movies with a large bubble remaining 2 or 3 seconds in the view field. All control parameters were kept constant, except for the LB area and the mean flow velocity  $v_0$ . The measured values of  $v(t)$  and  $D(t)$  were averaged over 5 images. When  $v(t) > 1.1 v_0$ , a flow is considered as being above the threshold, otherwise it is below. All experimental points are represented in the plane  $(h/D, \eta v_0 / \gamma)$  on Fig.5. Despite relatively large fluctuations, two distinct domains clearly appear on this phase diagram, corresponding to the two states, namely above or below the threshold (only the parameter ranges near the threshold were investigated).

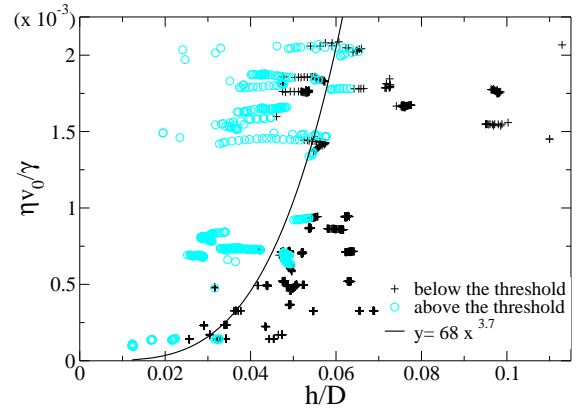


FIG. 5: Phase diagram of the large bubble instability. The control parameters are the capillary number built with the mean flow velocity  $Ca = \eta v_0 / \gamma$  and the LB diameter  $D$  adimensioned by the gap  $h$  between the plates. Each point of the graph corresponds to an image, on which the large bubble is migrating (circle) or not (cross). Despite large fluctuations, a frontier between the stable and unstable domains in the  $(Ca, h/D)$  plane can be determined. The full line is the best fit of this frontier in power law,  $a x^b$  with  $a$  and  $b$  adjustable.

To compare the experimental data presented on this figure 5 with the theoretical prediction given by eq. 4, an adjustment of the experimental frontier has been performed by minimization of the distances  $d_{front}$  between

the graph of a function and the experimental points located on the wrong side of this frontier. A least square method has been used with the set of functions  $f(x) = ax^b$ ,  $a$  and  $b$  being free parameters. We obtained thus the relation

$$\eta v_{th}/\gamma = 68 (h/D)^{3.7}. \quad (7)$$

The mean value of  $d_{front}$  increases of 10% if the exponent varies of  $\pm 0.5$ , which is the order of the precision on the exponent. This very crude estimation is nevertheless sufficient to discriminate between the two possible scaling for  $L_{geo}$ . Indeed,  $L_{geo} = D$  would correspond to an exponent 2 in eq.7 (with  $\alpha = 0.5$ ), whereas  $L_{geo} = d$  leads to the relation

$$\eta v_{th}/\gamma \sim (d/h)^2 (h/D)^4 \quad (8)$$

which is in better agreement with the relation 7. More experimental data would be needed to confirm the value of this exponent, but  $h$  can not be easily varied and  $d$  is confined to the small value range  $h < d \ll D \ll l$  with  $l$  the channel width. Nevertheless it tends to prove that  $L_{geo} \sim d$  and further modeling will therefore have to go beyond the continuum medium approximation, in which the bubble size  $d$  becomes irrelevant, and to take explicitly into account its discrete nature, at least in the high stress regions near the large bubble.

Above the threshold, the large bubble migrates through the foam with a velocity  $v(t) > v_0$ . Experimentally, the foam disorder induces large fluctuations of  $v$ , depicted on Fig. 4, which have been averaged out. The averages were performed over small bins of size  $\delta(\eta v_0/\gamma) = 0.25 \cdot 10^{-3}$  and  $\delta(h/D) = 0.01$  or  $0.02$ , leading to the graphs presented on Fig. 6. As expected, the large bubble velocity, in the frame of the foam, is vanishing at small foam velocity and/or small LB size. It can reach  $0.5v_0$  (*i.e*  $1.5v_0$  in the laboratory frame) for the largest foam flux explored. At larger velocities, images are not recorded fast enough by our camera to extract quantitative results. New physical processes, like films breakages, are involved and modify the dynamical behavior. For very large bubbles, the shape remains no more convex. The description of the phenomena in term of a Saffman Taylor instability is then probably more appropriate [14, 15].

The experimental data shown on Fig. 6 were rescaled according to the theoretical prediction eq. 6. The value used for the velocity threshold is the experimental fit given by eq. 7. We obtain in that way a good superposition of curves for the various  $h/D$  values, as well as an agreement with the theory (see Fig.4).

The problem of the orientation of the LB velocity remains open. Local crystallization is presumably important, as shown numerically. By contrast, disorder induces randomized plastic thresholds in the foam and thus creates most favorable paths for the LB migration that may deviate from a straight line. A precise analysis of the coupling between the local foam structure, the T1 local-

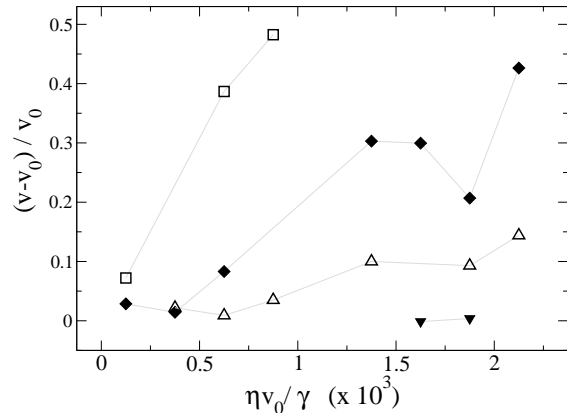


FIG. 6: Large bubble relative velocity  $(v-v_0)/v_0$  as a function of the mean foam velocity  $v_0$ , for different large bubble size  $D$  (the  $h/D$  ratio are given on Fig.7 with the same symbol convention). Each point represents an average over few tens of measures.

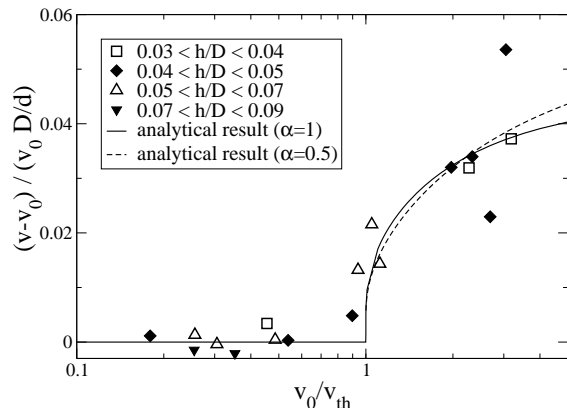


FIG. 7: Large bubble relative velocity in rescaled units (same data as in Fig. 6). The mean flow velocity threshold  $v_{th}(D)$  used to rescale the experimental data, is obtained from eq.7. The first analytical result (full line) is obtained from eq. 6, with the adjustable prefactor 0.045. Numerical simulations in vertex model have been performed, leading to a good agreement with theory as well, with an adjustable prefactor of 0.07 [9]. The second curve (dashed line) is the exact solution of eq. 5, using the experimental value of  $\alpha$  ( $\alpha = 0.5$ ), with an adjustable prefactor (see [9]).

ization and the LB shape and orientation might help to clarify these questions.

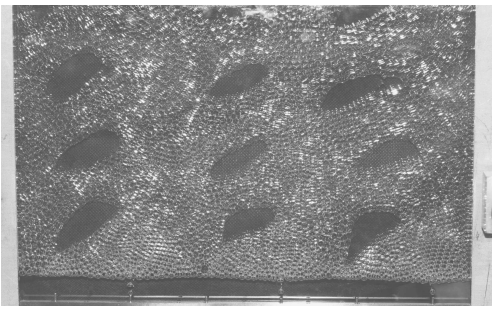


FIG. 8: Initial structure of the bidisperse foam.

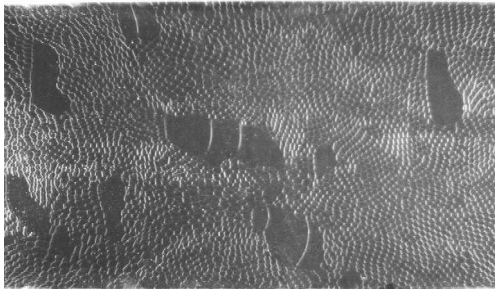


FIG. 9: Picture of the same foam as on Fig. 8, taken few seconds later, 50 cm downstream in the cell. The large bubbles have spontaneously organized in columns oriented along the flow.

## VI. LARGE BUBBLES SEGREGATION IN BIDISPERSE FOAM

Polydisperse foam flows imply obviously interactions between bubbles of various sizes. A mean field approach, in which we would consider that each bubble migrates in an effective continuous medium and adjusts its velocity as a function of its own size and of the local mean velocity and mean bubble size does not seem appropriate. The flow appears indeed to be dominated by correlations between bubbles. In this last part, we point out the attractive interactions between a set of large bubbles, and their spontaneous organization in columns.

A regular network of approximately 10 large bubbles is initially produced in a monodisperse foam, at rest (Fig. 8). The middle of this network is used as abscissa reference ( $x = 0$ ). Then the flow is turned on, at a velocity higher than the threshold, and the large bubbles begin to migrate through the foam. When two large bubbles meet, they migrate together. This aggregation leads progressively to large bubbles domains of increasing size, organised in one bubble width columns, oriented along the flow (see Fig. 9). The length of the columns was measured at two points along the flow, for ten flows (99 bubbles). The number  $N(n)$  of bubbles involved in a  $n$ -bubbles column when crossing the abscissas  $x = 50$  or  $x = 100$  cm is plotted for each value of  $n$  on Fig. 10 ( $n = 1$  for an isolated bubble). It represents equivalently the number of

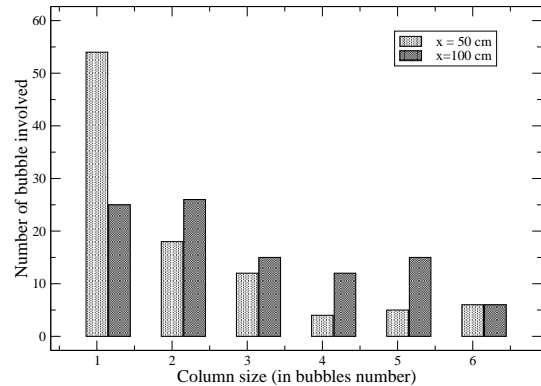


FIG. 10: Large bubbles repartition in the columns of various sizes, at two abscissa in the cell. Ten flows have been recorded, involving 99 large bubbles. The position  $x = 0$  corresponds to the mean abscissa of the initial regular large bubble network (see Fig. 8). Each time a large bubble crosses the line  $x = 50$  cm (resp.  $x = 100$  cm), the size of the column in which this bubble migrates is recorded (size 1 corresponds to an isolated large bubble) and the obtained distribution is plotted. The count is focused on the bubbles, which number is conserved, and the  $n$ -bubbles columns are thus counted  $n$  times.

$n$ -bubbles columns, with a weight  $n$ . The initial distribution at  $x = 0$  is simply  $N(1) = 99$  and  $N(i) = 0$  for  $i > 1$ . In order to follow every large bubble, we needed a large field of view. The image quality is therefore reduced and the analysis was done by hand.

The number of isolated bubbles decreases along the flow. The aggregation process may be due to attractive forces, or simply due to the spontaneous fluctuations of the large bubbles trajectories. Indeed, once in contact, two large bubbles never unbind, which leads to an effective attractive interaction, even without long range attractive forces. The orientation of the domains is probably governed by the same phenomenon as in viscous digitation.

## VII. CONCLUSION

In conclusion, the reported experiments evidence the crucial role of polydispersity in non quasi-static foam flows and open a whole field of investigations. We measured the relative velocity of a single large bubble created in a monodisperse foam as a function of its size and of the mean flow velocity. The results are explained with non trivial scaling arguments. In a bidisperse foam, we show that the large bubbles are attracted to each other and organise themselves in columns oriented along the flow. A deeper analysis of the velocity fields around these large bubbles will allow for a better understanding of the nature of the attractive interaction. Strong spatial correla-

tions are observed and a mean field approach is probably not enough to explain the velocity field of a fully poly-disperse foam.

The dissipation is of different nature in three-dimensional foams. Nevertheless, it is still localized in the liquid phase, and the largest bubbles remain easier to deform or displace. Similar destabilizations are thus

expected to occur in non quasi-static 3D flows and might have important practical consequences.

**Acknowledgments:** We thank *Rennes Métropole* and CNRS for financial support, P. Chasles and S. Bourlès for technical assistance and valuable advices and G. Le Caër and B. Dollet for enlightening discussions.

- 
- [1] M. A. Fortes and M. E. Rosa, J. Phys.: Condens. Matter **11**, 7947 (1999).
  - [2] G. Debregeas, H. Tabuteau, and J.-M. diMeglio, Phys. Rev. Lett. **87**, 178305 (2001).
  - [3] J. Lauridsen, M. Twardos, and M. Dennin, Phys. Rev. Lett. **89**, 098303 (2002).
  - [4] M. Asipauskas, M. Aubouy, J. A. Glazier, F. Graner, and Y. Jiang, Granular Matter **5**, 71 (2003).
  - [5] G. Hirasaki and J. B. Lawson, Soc. Pet. Eng. J. , p. 176 (1985).
  - [6] I. Cantat, N. Kern, and R. Delannay, Europhys. Lett. **65**, 726 (2004).
  - [7] D. Weaire and S. Hutzler, *The physics of foams* (University press, Oxford, 2000).
  - [8] I. Cantat and R. Delannay, Phys. Rev. E **67**, 031501 (2003).
  - [9] I. Cantat and R. Delannay, Eur. Phys. J. E , (to appear) (2005).
  - [10] F. P. Bretherton, J. Fluid Mech. **10**, 166 (1961).
  - [11] N. D. Denkov, V. Subramanian, D. Gurovich, and A. Lips, preprint (2005).
  - [12] B. Dollet *et al.*, Phys. Rev. E **71**, 031403 (2005).
  - [13] D. Weaire and M. A. Fortes, Adv. Phys. **43**, 685 (1994).
  - [14] S. S. Park and D. J. Durian, Phys. Rev. Lett. **72**, 3347 (1994).
  - [15] A. Lindner, P. Coussot, and D. Bonn, Phys. Rev. Lett. **85**, 314 (2000).